Local photoemission spectra and effects of spatial inhomogeneity in the BCS-BEC-crossover regime of a trapped ultracold Fermi gas

Miki Ota,[1] Hiroyuki Tajima,[2] Ryo Hanai,[2] Daisuke Inotani,[2] and Yoji Ohashi[2]
[1]*INO-CNR BEC Center and Dipartimento di Fisica, Università di Trento, 38123 Povo, Italy*
[2]*Department of Physics, Keio University, 3-14-1 Hiyoshi, Kohoku-ku, Yokohama 223-8522, Japan*
(Received 3 March 2017; published 22 May 2017)

We theoretically investigate single-particle excitations in the BCS-BEC-crossover regime of an ultracold Fermi gas. Including strong pairing fluctuations within a T-matrix approximation, as well as effects of a harmonic trap potential in the local-density approximation, we calculate the local photoemission spectrum in the normal state. Recently, the JILA group measured this quantity in a ^{40}K Fermi gas in order to examine *homogeneous* single-particle properties of this system. Comparing our results with this experiment, we show that this attempt indeed succeeds under JILA's experimental condition. However, we also find that the current local photoemission spectroscopy still has room for improvement in order to examine the pseudogap phenomenon predicted in the BCS-BEC-crossover region. Since ultracold Fermi gases are always in a trap, our results would be useful in applying this system to various *homogeneous* Fermi systems as a quantum simulator.

DOI: 10.1103/PhysRevA.95.053623

I. INTRODUCTION

While the high tunability of various physical parameters is an advantage of an ultracold Fermi gas [1–4], the spatial inhomogeneity of a trap potential may be a weak point of this many-body system, especially when one tries to use it as a quantum simulator for other *uniform* Fermi systems. Using a tunable interaction associated with a Feshbach resonance [4,5], we can now study superfluid properties of ^{40}K and ^{6}Li Fermi gases at various interaction strengths in a systematic manner [6–9]. Thus, when the above-mentioned weak point is overcome, one would be able to concentrate on the so-called BCS-BEC-crossover phenomenon [1,10–17] without being annoyed by the unwanted spatial inhomogeneity. Since understanding strong correlations is crucial in various Fermi systems, such as high-T_c cuprates [18–21], as well as neutron stars [22], such an improvement would also make an impact on these fields.

So far, several ideas have been proposed and developed to overcome this problem. One idea is to use the combined Gibbs-Duhem equation with the local-density approximation (LDA) [23], which enables us to evaluate the pressure P of a *uniform* Fermi gas from the observed density profile in a *trapped* Fermi gas. Then, we can determine other thermodynamic quantities in a uniform Fermi gas from P by way of appropriate thermodynamic identities. This method is now widely used in cold Fermi gas physics [24–26].

To suppress the effects of a harmonic potential, the nonharmonic trap potential has also been tested [27,28]. Very recently, for a ^{6}Li Fermi gas in a cylindrical trap potential (where atoms feel an almost uniform potential in the central region), Zwierlein and coworkers have measured the atomic momentum distribution to observe a clear signature of the Fermi surface formation below the Fermi temperature T_F [28].

In addition to these, Jin and coworkers have recently invented a local photoemission-type spectroscopy (LPES) [29]. While the previous photoemission-type spectroscopy (PES) has no spatial resolution [30,31], LPES employs a space-selective imaging technique [32–34] to observe only single-particle excitations around the trap center (where the effects of a harmonic trap are weak). Since the combined Gibbs-Duhem equation with LDA is valid only for thermodynamic quantities, LPES is expected to contribute to the understanding of *excitation* properties of a uniform Fermi gas in the crossover region.

Figure 1 schematically shows the difference between PES and LPES. In PES [30,31,35,36], rf photons are applied to the whole gas cloud to transfer atoms in the $|\uparrow\rangle$ state to the third one, $|3\rangle$, as shown in Fig. 1(a). The photoemission spectrum is then obtained by probing $|3\rangle$ using a time-of-flight (TOF) technique. In LPES [29], on the other hand, before TOF measurement, additional hollow light beams are applied to the system [Fig. 1(b)] to selectively excite $|3\rangle$-state atoms around the edge of the gas cloud to the fourth state $|4\rangle$ [LPES in Fig. 1(a)]. When $|4\rangle$ is chosen to be invisible in the successive TOF measurement, LPES can selectively probe atoms in the trap center.

Because of this advantage, LPES is also expected to be able to resolve a long-standing debate on the pseudogap problem in this field. Since pairing fluctuations are strong in the BCS-BEC-crossover region, the formation of preformed Cooper pairs, as well as the associated pseudogap phenomenon [where a gaplike structure appears in the single-particle density of states (DOS) in the normal state], has theoretically been predicted [37–43]. Experimentally, although the direct observation of the DOS is still difficult in cold Fermi gas physics, a recent PES experiment on a ^{40}K Fermi gas [30,31] found an anomalous spectral structure which is consistent with the prediction [37–43]. However, it has also been argued that the observed anomaly is not a signature of pseudogap but simply comes from the spatial inhomogeneity of a trapped Fermi gas [44,45], so that the existence of this many-body phenomenon is still controversial. To resolve this debate, LPES is very promising because this experiment can, in principle, eliminate the effects of a trap from the spectrum. Since the pseudogap phenomenon has also been discussed in high-T_c cuprates as a key to clarify the pairing mechanism [14,46–50], the observation of pseudogap in the simpler gas system would also contribute to the study of this more complicated electron system.

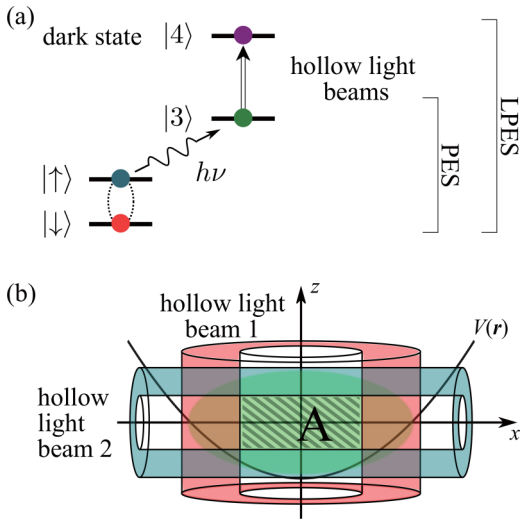

FIG. 1. Schematic explanation for the local photoemission spectroscopy (LPES). (a) In the ordinary PES, rf photons are applied to a Fermi gas consisting of two atomic hyperfine states ($|\sigma\rangle = |\uparrow,\downarrow\rangle$), which excite $|\uparrow\rangle$-state atoms to the third state $|3\rangle$. In LPES, after this process, additional hollow light beams are applied to the gas [see (b)] to further excite $|3\rangle$-state atoms around the edge of the gas cloud to the fourth state $|4\rangle$. Here, $|4\rangle$ is a dark state in the sense that it is invisible in TOF measurement. (b) This additional manipulation enables LPES to selectively observe single-particle excitations in the central region (labeled "A").

In the recent LPES experiment on a ^{40}K Fermi gas [29], the observed spectrum is similar to the previous PES result [30,31], which seems to support the pseudogap scenario. However, because the current LPES [29] still needs at least about 30% of the trapped atoms to obtain detectable spectral intensity, it must be done not at the trap center, but for a finite volume fraction around the trap center. Thus, it is still unclear whether the observed LPES spectra really describe single-particle properties of a *homogeneous* system or still involve non-negligible inhomogeneous effects of a harmonic trap.

The purpose of this paper is to theoretically investigate the LPES in the BCS-BEC-crossover regime of a trapped normal Fermi gas. Including pairing fluctuations in the BCS-BEC-crossover region within the framework of a strong-coupling T-matrix approximation (TMA), as well as the effects of a harmonic trap within the LDA, we assess to what extent LPES can eliminate the effects of a harmonic trap from the photoemission spectrum. We clarify the region where the current LPES technique can obtain single-particle properties of a *uniform* Fermi gas in the phase diagram with respect to the temperature and the strength of the pairing interaction. We also discuss how the local photoemission spectrum is sensitive to detailed spatial selection.

This paper is organized as follows. In Sec. II, we explain our formulation. In addition to the combined TMA with LDA to describe a trapped Fermi gas in the BCS-BEC-crossover region, we also explain how to theoretically evaluate the local photoemission spectrum. In Sec. III, we show our numerical results. We compare calculated spectra with the recent experiment on a ^{40}K Fermi gas [29]. Throughout this paper, we set $\hbar = k_B = 1$ for simplicity. In the uniform case, the system volume V is taken to be unity.

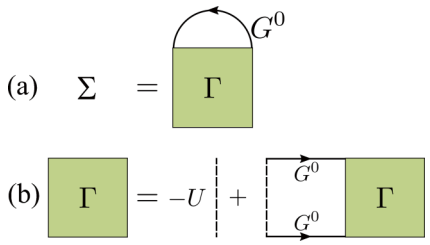

FIG. 2. (a) TMA self-energy $\Sigma(\boldsymbol{p},i\omega_n)$. The particle-particle scattering matrix $\Gamma(\boldsymbol{q},i\nu_n)$ is given by the sum of the ladder diagrams shown in (b). $G^0 = 1/[i\omega_n - \xi_{\boldsymbol{p}}]$ is the bare single-particle Green's function. $-U(<0)$ is a pairing interaction.

II. FORMULATION

We start from a two-component Fermi gas described by the model Hamiltonian,

$$H = \sum_{\boldsymbol{p},\sigma} \xi_{\boldsymbol{p}} c^\dagger_{\boldsymbol{p},\sigma} c_{\boldsymbol{p},\sigma} - U \sum_{\boldsymbol{p},\boldsymbol{p}',\boldsymbol{q}} c^\dagger_{\boldsymbol{p}+\boldsymbol{q},\uparrow} c^\dagger_{\boldsymbol{p}'-\boldsymbol{q},\downarrow} c_{\boldsymbol{p}',\downarrow} c_{\boldsymbol{p},\uparrow}. \tag{1}$$

We first explain TMA formalism and PES expression in the *uniform* case. Later, we will explain how to incorporate the effects of a harmonic trap into the theory within LDA. In Eq. (1), $c^\dagger_{\boldsymbol{p},\sigma}$ is the creation operator of a Fermi atom in the hyperfine state described by pseudospin $\sigma = \uparrow,\downarrow$. $\xi_{\boldsymbol{p}} = \varepsilon_{\boldsymbol{p}} - \mu = \boldsymbol{p}^2/(2m) - \mu$ is the kinetic energy, measured from the Fermi chemical potential μ, where m is an atomic mass. $-U(<0)$ is an attractive pairing interaction, which is assumed to be tunable by a Feshbach resonance technique [4]. As usual, we measure the interaction strength in terms of the observable s-wave scattering length a_s, which is related to $-U$ as

$$\frac{4\pi a_s}{m} = -\frac{U}{1 - U\sum_{\boldsymbol{p}}^{p_c} 1/(2\varepsilon_{\boldsymbol{p}})}, \tag{2}$$

where p_c is a momentum cutoff.

Strong-coupling corrections to single-particle excitations are conveniently described by the self-energy $\Sigma(\boldsymbol{p},i\omega_n)$ in the single-particle thermal Green's function [51,52],

$$G(\mathbf{p},i\omega_n) = \frac{1}{i\omega_n - \xi_{\boldsymbol{p}} - \Sigma(\boldsymbol{p},i\omega_n)}, \tag{3}$$

where ω_n is the fermion Matsubara frequency. In this paper, we deal with the self-energy correction $\Sigma(\boldsymbol{p},i\omega_n)$ within the TMA [14,15,37,38], which is diagrammatically given in Fig. 2. We briefly note that TMA can describe the BCS-BEC-crossover behavior of T_c, as well as the pseudogapped density of states in the crossover region [14,15,37,38]. This strong-coupling theory has also been used to calculate the conventional PES [53] to successfully explain the observed spectra in a ^{40}K Fermi gas [30,31]. Thus, we expect that TMA is also suitable for our purpose.

We note, however, that TMA cannot correctly describe all the strong-coupling phenomena in the BCS-BEC-crossover

region. For example, in the superfluid phase, TMA is known to overestimate the effective interaction between pairs in the strong-coupling Bose-Einstein-condensate (BEC) regime, giving a larger value ($a_B = 2a_s$) of the molecular scattering length than the correct one, $a_B = 0.6a_s$ [54,55]. It has also been pointed out that TMA unphysically gives negative spin susceptibility in the BCS-BEC-crossover region [56]. Thus, although TMA seems valid for the study of PES as mentioned previously, this strong-coupling theory still has room for improvement from the general viewpoint of BCS-BEC-crossover physics.

The summation of the TMA diagrams in Fig. 2 gives

$$\Sigma(\boldsymbol{p},i\omega_n) = T\sum_{\boldsymbol{q},i\nu_n}\Gamma(\boldsymbol{q},i\nu_n)G^0(\boldsymbol{q}-\boldsymbol{p},i\nu_n - i\omega_n). \tag{4}$$

Here, $i\nu_n$ is the boson Matsubara frequency, and $G^0(\boldsymbol{p},i\omega_n) = 1/[i\omega_n - \xi_{\boldsymbol{p}}]$ is the bare single-particle Green's function. In Eq. (4), the particle-particle scattering matrix,

$$\Gamma(\boldsymbol{q},i\nu_n) = -\frac{U}{1-U\Pi(\boldsymbol{q},i\nu_n)}, \tag{5}$$

describes fluctuations in the Cooper channel, where

$$\begin{aligned}\Pi(\boldsymbol{q},i\nu_n) &= T\sum_{\boldsymbol{p},\omega_n} G^0(\boldsymbol{p}+\boldsymbol{q}/2,i\omega_n + i\nu_n)\\ &\quad\times G^0(-\boldsymbol{p}+\boldsymbol{q}/2,-i\omega_n)\\ &= \sum_{\boldsymbol{p}}\frac{1-f(\xi_{\boldsymbol{p}+\boldsymbol{q}/2})-f(\xi_{-\boldsymbol{p}+\boldsymbol{q}/2})}{\xi_{\boldsymbol{p}+\boldsymbol{q}/2}+\xi_{-\boldsymbol{p}+\boldsymbol{q}/2}-i\nu_n}\end{aligned} \tag{6}$$

is the lowest-order pair-correlation function, with $f(x)$ being the Fermi distribution function. As usual, the momentum summation in Eq. (6) involves the ultraviolet divergence, which, however, does not affect the final result when the interaction strength is measured in terms of the s-wave scattering length a_s as

$$\Gamma(\boldsymbol{q},i\nu_n) = \frac{\frac{4\pi a_s}{m}}{1+\frac{4\pi a_s}{m}\left[\Pi(\boldsymbol{q},i\nu_n) - \sum_{\boldsymbol{p}}\frac{1}{2\varepsilon_{\boldsymbol{p}}}\right]}. \tag{7}$$

To describe excitations from $|\uparrow\rangle$ to $|3\rangle$ by rf photons [30,31], we add the corresponding Hamiltonian [35,57–60],

$$\begin{aligned}H_3 &= \sum_{\boldsymbol{p}}[\varepsilon_{\boldsymbol{p}} + \omega_3 - \mu_3]b^\dagger_{\boldsymbol{p}}b_{\boldsymbol{p}}\\ &\quad + t_{\rm rf}\sum_{\boldsymbol{p}}[e^{-i\omega_{\rm L}t}b^\dagger_{\boldsymbol{p}+\boldsymbol{q}_{\rm L}}c_{\boldsymbol{p},\uparrow} + {\rm H.c.}],\end{aligned} \tag{8}$$

to our model in Eq. (1). In Eq. (8), $b^\dagger_{\boldsymbol{p}}$ is the creation operator of a Fermi atom in $|3\rangle$ with the kinetic energy $\varepsilon_{\boldsymbol{p}} + \omega_3 - \mu_3$, measured from the chemical potential μ_3 (where ω_3 is the energy difference between $|\uparrow\rangle$ and $|3\rangle$). The last term in Eq. (8) ($\equiv H_{\rm T}$) describes photon-assisted tunneling between $|\uparrow\rangle$ and $|3\rangle$ in the rotating-wave approximation [35,57–61], where $t_{\rm rf}$ is the transfer-matrix element between the two states, and $\boldsymbol{q}_{\rm L}$ and $\omega_{\rm L}$ are the momentum and energy of the rf photon, respectively.

The tunneling current $I(\boldsymbol{p},t)$ from $|\uparrow\rangle$ to $|3\rangle$ is given as the increase rate of the number $N_3(\boldsymbol{p},t)$ of $|3\rangle$-state atoms with momentum $\boldsymbol{p}$. Treating the tunneling Hamiltonian $H_{\rm T}$ within the linear response theory [51], one obtains

$$I(\boldsymbol{p},t) = \langle\dot{N}_3(\boldsymbol{p},t)\rangle = i\int_{-\infty}^{t}dt'\langle[H_{\rm T}(t'),\hat{I}(\boldsymbol{p},t)]\rangle, \tag{9}$$

where

$$\hat{I}(\boldsymbol{p},t) = \dot{N}_3(\boldsymbol{p},t) = -it_{\rm rf}[e^{-i\omega_{\rm L}t}b^\dagger_{\boldsymbol{p}+\boldsymbol{q}_{\rm L}}(t)c_{\boldsymbol{p},\uparrow}(t) - {\rm H.c.}] \tag{10}$$

is a current operator, with $H_{\rm T}(t') = e^{iHt'}H_{\rm T}e^{-iHt'}$. The photoemission spectrum $I(\boldsymbol{p},\omega)$ is given as the Fourier-transformed tunneling current $I(\boldsymbol{p},t)$ in terms of the time variable t. Assuming that the photon momentum $\boldsymbol{q}_{\rm L}$ is negligibly small and the third state $|3\rangle$ is initially vacant [$f(\varepsilon_{\boldsymbol{p}} + \omega_3 - \mu_3) = 0$], we have

$$I(\boldsymbol{p},\Omega) = 2\pi t_{\rm rf}^2 A(\boldsymbol{p},\xi_{\boldsymbol{p}} - \Omega)f(\xi_{\boldsymbol{p}} - \Omega). \tag{11}$$

Here, $\Omega \equiv \omega_3 + \mu_3 - \mu - \omega_{\rm L}$ is sometimes referred to as the detuning frequency in the literature. Equation (11) involves the single-particle spectral weight $A(\boldsymbol{p},\omega)$, which is related to the analytic continued single-particle Green's function in Eq. (3) as

$$A(\boldsymbol{p},\omega) = -\frac{1}{\pi}{\rm Im}[G(\boldsymbol{p},i\omega_n \to \omega + i\delta)], \tag{12}$$

where δ is an infinitesimally small positive number. Thus, the photoemission spectrum $I(\boldsymbol{p},\Omega)$ in Eq. (11) gives us useful information about many-body corrections to single-particle excitations in the BCS-BEC-crossover region.

We now include the effects of a harmonic trap. In LDA, this extension is achieved by simply replacing μ and μ_3 by the position-dependent ones, $\mu(\mathbf{r}) = \mu - V(\mathbf{r})$ and $\mu_3(\mathbf{r}) = \mu_3 - V(\mathbf{r})$, respectively [53,62–64]. Here,

$$V(\boldsymbol{r}) = \tfrac{1}{2}m\omega_{\rm tr}^2 r^2 \tag{13}$$

is a harmonic potential with trap frequency $\omega_{\rm tr}$ [65]. Equations (3)–(7) then depend on $\boldsymbol{r}$ through $\mu(\boldsymbol{r})$. For example, the LDA single-particle thermal Green's function has the form

$$G(\boldsymbol{p},i\omega_n,\boldsymbol{r}) = \frac{1}{i\omega_n - \xi_{\boldsymbol{p}}(\boldsymbol{r}) - \Sigma(\boldsymbol{p},i\omega_n,\boldsymbol{r})}, \tag{14}$$

where $\xi_{\boldsymbol{p}}(\boldsymbol{r}) = \varepsilon_{\boldsymbol{p}} - \mu(\boldsymbol{r})$. The LDA photoemission spectrum is given by

$$I(\boldsymbol{p},\Omega,\boldsymbol{r}) = 2\pi t_{\rm rf}^2 A(\boldsymbol{p},\xi_{\boldsymbol{p}}(\boldsymbol{r}) - \Omega,\boldsymbol{r})f(\xi_{\boldsymbol{p}}(\boldsymbol{r}) - \Omega), \tag{15}$$

where $A(\boldsymbol{p},\omega,\boldsymbol{r}) = -{\rm Im}[G(\boldsymbol{p},i\omega \to \omega + i\delta,\boldsymbol{r})]/\pi$. We briefly note that Ω in Eq. (15) is still $\boldsymbol{r}$ independent in LDA.

We briefly note that LDA physically corresponds to dividing a gas cloud into a set of many locally homogeneous systems, which are independent of one another. This approximation is valid for the case when each local system has a large number of atoms and when the spatial dependence of the harmonic potential is negligible in each local system. While these conditions are satisfied around the trap center, this local approximation becomes doubtful around the edge of the gap (where the particle density is low and the spatial variation of a harmonic trap is remarkable) [66]. In this regard, the LPES selectively detects spectral information in the central region

[see Eq. (17)], so that we can safely use LDA to study this local quantity.

In the conventional PES with no spatial resolution [30,31], the spectrum $I_{\rm PES}(\boldsymbol{p},\omega)$ is obtained from the spatial average of Eq. (15) over the *entire* gas cloud. When we slightly modify the expression so that we can directly compare our results with experimental data, we have

$$I_{\rm PES}(\boldsymbol{p},\omega) = \frac{2\pi t_{\rm rf}^2}{V} p^2 \int d\boldsymbol{r}\, A(\boldsymbol{p},\omega-\mu(\boldsymbol{r}),\boldsymbol{r}) f(\omega-\mu(\boldsymbol{r})). \tag{16}$$

Here, $V = 4\pi R_{\rm F}^3/3$ is a characteristic volume of the gas cloud, where $R_{\rm F} = (24Nk_{\rm F}^{-3})^{1/3}$ is the Thomas-Fermi radius [66] (where N and $k_{\rm F}$ are the number of Fermi atoms and the Fermi momentum in the trap center in LDA, respectively). In obtaining Eq. (16), we have changed the variable as $\Omega = \xi_{\boldsymbol{p}} - \omega$ and have multiplied the spectrum by p^2, following the PES experiment [30,31].

As mentioned in Sec. I, the LPES developed by the JILA group [29] uses a space-selective imaging technique [32–34]. This can be conveniently incorporated into the theory by inserting a "space-selective function" $P(\boldsymbol{r})$, which describes the probability that a $|3\rangle$-state atom at $\boldsymbol{r}$ is *not* scattered into $|4\rangle$, into the PES expression in Eq. (16). The resulting LPES spectrum is given by

$$I_{\rm LPES}(\boldsymbol{p},\omega) = \frac{2\pi t_{\rm rf}^2}{V} p^2 \int d\boldsymbol{r}\, A(\boldsymbol{p},\omega-\mu(\boldsymbol{r}),\boldsymbol{r}) \times f(\omega-\mu(\boldsymbol{r}))P(\boldsymbol{r}). \tag{17}$$

In the JILA experiment [29], the space selection was done using two hollow light beams, both of which have a second-order Laguerre-Gaussian profile [32], to kick atoms in the outer region of the gas cloud out to the invisible $|4\rangle$ state (see Fig. 1). To model this setup, we take [67]

$$P(\boldsymbol{r}) = e^{-\frac{J(r)}{w}}, \tag{18}$$

where

$$J(r) = J_0\left(\frac{2r^2}{w^2}\right)^2 e^{-\frac{2r^2}{w^2}}, \tag{19}$$

with J_0 and w describing the power and the waist of the beam, respectively. For clarity, we show a detailed spatial variation of $P(\boldsymbol{r})$ in Fig. 3. We briefly note that, although $P(\boldsymbol{r})$ in Eq. (18) does not exactly reproduce the experimental setup [with two hollow light beams; see Fig. 1(b)] [29,67], we will later show that the LPES spectrum is actually not so sensitive to the detailed spatial variation of $P(\boldsymbol{r})$.

In this paper, we also consider the case with a *sharp* cutoff,

$$P(\boldsymbol{r}) = \Theta(R_{\rm cut} - r), \tag{20}$$

where $\Theta(x)$ is the step function and $R_{\rm cut}$ is a cutoff radius.

Before ending this section, we comment on our numerical calculations. We first determine the Fermi chemical potential $\mu(T)$ in the normal state from the LDA number equation [63],

$$N = 2T \int d\boldsymbol{r} \sum_{\boldsymbol{p},i\omega_n} e^{i\omega_n\delta} G(\boldsymbol{p},i\omega_n,\boldsymbol{r}). \tag{21}$$

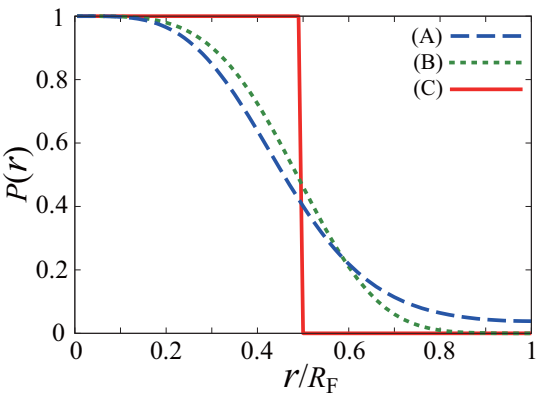

FIG. 3. Space-selective function $P(r)$ in Eq. (18) as a function of r. For curve A $w/R_{\rm F} = 1$ and $J_0/R_{\rm F}^2 = 6$. This parameter set is used in Fig. 4(a). For curve B $w/R_{\rm F} = 3$ and $J_0/R_{\rm F}^2 = 2380$. Curve C shows the case with a sharp cutoff in Eq. (20) with $R_{\rm cut}/R_{\rm F} = 0.48$. This case is examined in Fig. 4(c). In all three cases, when one considers the case shown in Fig. 4, 30% of trapped atoms contribute to the local photoemission spectrum.

Using the calculated $\mu(T)$, we evaluate the local photoemission spectrum $I_{\rm LPES}(\boldsymbol{p},\omega)$ in Eq. (17). For this purpose, we numerically execute the analytic continuation $G(\boldsymbol{p},i\omega_n \to \omega + i\delta,\boldsymbol{r})$ in the Padé approximation [68,69] to evaluate the spectral weight $A(\boldsymbol{p},\omega,\boldsymbol{r})$ in Eq. (17). In this paper, we focus on the normal state above the superfluid phase transition temperature $T_{\rm c}$. In LDA, $T_{\rm c}$ is determined as the temperature at which the Thouless criterion [70] is satisfied at the trap center ($\boldsymbol{r} = 0$) [63], that is,

$$\Gamma(\boldsymbol{q} = \boldsymbol{0}, i\nu_n = 0, \boldsymbol{r} = \boldsymbol{0})^{-1} = 0. \tag{22}$$

This condition gives the same form as the ordinary $T_{\rm c}$ equation in the BCS theory,

$$1 = -\frac{4\pi a_s}{m} \sum_{\boldsymbol{p}} \left[\frac{1}{2\xi_{\boldsymbol{p}}} \tanh\frac{\xi_{\boldsymbol{p}}}{2T_{\rm c}} - \frac{1}{2\varepsilon_{\boldsymbol{p}}}\right]. \tag{23}$$

As usual, we numerically solve Eq. (23) together with the number equation (21) to self-consistently determine $T_{\rm c}$ and $\mu(T_{\rm c})$.

III. LOCAL PHOTOEMISSION SPECTRA IN THE BCS-BEC-CROSSOVER REGION

Figure 4(a) shows the calculated intensity $I_{\rm LPES}(\boldsymbol{p},\omega)$ of the local photoemission spectrum in the unitary regime of an ultracold Fermi gas at $T = 1.24T_{\rm c}$. In this figure, 30% of the trapped atoms in the central region are selectively probed. We find that the overall structure of the spectral intensity $I_{\rm LPES}(\boldsymbol{p},\omega)$ agrees well with the recent LPES experiment on a ^{40}K Fermi gas [Fig. 4(b)] [29]. In particular, our result quantitatively explains the back-bending behavior of the observed spectral peak [white circles in Figs. 4(a) and 4(b); see the black solid line in Fig. 4(a)]. Such agreements are also obtained at different interaction strengths in the crossover region, although we do not explicitly show them in this paper. These agreements confirm the validity of our approach in this regime.

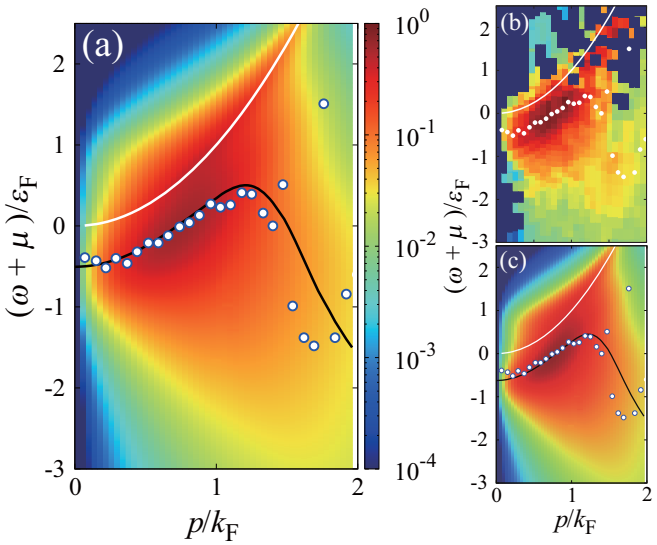

FIG. 4. Comparison of (a) the calculated intensity $I_{\rm LPES}(\boldsymbol{p},\omega)$ of the local photoemission spectrum (with (b) the recent experiment on a ^{40}K Fermi gas [29]. Both are in the unitary regime $[(k_F a_s)^{-1}=0.1]$ at $T/T_c=1.24$, and 30% of atoms in the trap center contribute to the spectrum. To realize this situation, we set $w/R_F=1$ and $J_0/R_F^2=6$ in (a) (curve A in Fig. 3). (c) Calculated spectral intensity in the case of a sharp cutoff in Eq. (20). To reproduce the experimental probing rate (30%), we set $R_{\rm cut}/R_F=0.48$ (curve C in Fig. 3). The other parameters are the same as those in (a) and (b). In these plots, the black solid lines and white circles show the peak positions of the calculated and observed spectral intensities, respectively. The white solid line shows the free-particle dispersion, $\omega+\mu=\boldsymbol{p}^2/(2m)$. The spectral intensity is normalized by $(k_F\varepsilon_F)^{-1}\int_{-\mu-5\varepsilon_F}^{-\mu+4\varepsilon_F}d\omega\int_0^{2k_F}dp\,I_{\rm LPES}(\boldsymbol{p},\omega)$, where ε_F and k_F are the Fermi energy and the Fermi momentum in LDA, respectively.

Figure 4(c) shows the case when 30% of the atoms are selected by the sharp cutoff function in Eq. (20), which gives almost the same result as Fig. 4(a). We also see in Fig. 5 that, although the parameter set (w,J_0) in $P(\boldsymbol{r})$ in Eq. (18) which probes 30% of the atoms is not unique, the spectral peak line is not sensitive to this ambiguity. This result indicates that, once the probing rate ($\equiv N_{\rm prob}/N$) is fixed, the detailed spatial selection is not so crucial for the local photoemission spectrum.

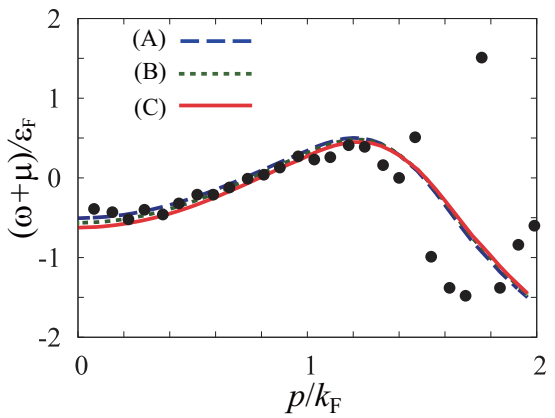

FIG. 5. Calculated spectral peak lines in cases A–C in Fig. 3. We take $(k_F a_s)^{-1}=0.1$, $T=1.24T_c$, and $N_{\rm prob}/N=0.3$. Curves A and C are the same cases as in Figs. 4(a) and 4(c), respectively. Solid circles are experimental data [29].

To assess to what extent LPES detects single-particle properties of a uniform Fermi gas from a trapped Fermi gas, we conveniently introduce the quantity

$$h=\sum_{\boldsymbol{p}}\int d\omega\langle\langle I_{\rm uniform}(\boldsymbol{p},\omega)/p^2\rangle\rangle\langle\langle I_{\rm LPES}(\boldsymbol{p},\omega)/p^2\rangle\rangle, \tag{24}$$

where $I_{\rm uniform}(\boldsymbol{p},\omega)$ is the photoemission spectrum in a uniform Fermi gas with the same temperature and interaction strength as in the trapped case. The atomic number density in this uniform case is chosen to be equal to the central density in the trapped case. In the present formalism, $I_{\rm uniform}(\boldsymbol{p},\omega)$ is given by

$$I_{\rm uniform}(\boldsymbol{p},\omega)=2\pi t_{\rm rf}^2 p^2 A(\boldsymbol{k},\omega-\mu,\boldsymbol{r}=0)f(\omega-\mu). \tag{25}$$

In Eq. (24), $\langle\langle X(\boldsymbol{p},\omega)\rangle\rangle$ means the normalization

$$\langle\langle X(\boldsymbol{p},\omega)\rangle\rangle=\frac{X(\boldsymbol{p},\omega)}{\sqrt{\sum_{\boldsymbol{p}}\int d\omega X^2(\boldsymbol{p},\omega)}}. \tag{26}$$

We note that one obtains $h=1$ when the local photoemission spectrum $I_{\rm LPES}(\boldsymbol{p},\omega)$ is the same as the uniform result $I_{\rm uniform}(\boldsymbol{p},\omega)$. The decrease from unity ($h<1$) means that the spectrum is still influenced by spatial inhomogeneity by a harmonic trap.

Figures 6(a)–6(d) show how the probing rate $N_{\rm prob}/N$ affects $I_{\rm LPES}(\boldsymbol{p},\omega)$ when $(k_F a_s)^{-1}=0.1$ and $T=1.24T_c$. The spectral structure in the experimental situation [Fig. 6(c)] appears closer to the uniform result in Fig. 6(a) than the conventional PES case in Fig. 6(d) (where all the atoms in the trap contribute to the spectrum). Indeed, the value $h=0.92$ in the case of Fig. 6(c) is very close to unity. In this sense, the space-selective imaging technique in the recent LPES experiment on a ^{40}K Fermi gas [29] is considered to succeed in observing single-particle excitations in a (nearly) uniform Fermi gas.

However, we point out that the current experimental limitation $N_{\rm prob}/N\gtrsim 0.3$ is not always enough to obtain single-particle properties of a *uniform* Fermi gas. For example, in the unitarity limit at T_c, Fig. 6(g) shows that the similarity of the spectrum to the uniform result is at most $h=0.69\ll 1$. Indeed, we see in Fig. 6(g) that the spectrum has a large intensity around the free-particle dispersion (white solid line), compared to the uniform case in Fig. 6(e). This structure is rather close to the PES case shown in Fig. 6(h). To obtain $h=0.92$ in this case, one needs to tune the probing rate down to $N_{\rm prob}/N=0.03$ [Fig. 6(f)], which is, however, beyond the current experimental limitation.

These results indicate that, not only the probing rate $N_{\rm prob}/N$ but also the temperature is crucial to obtain $h\simeq 1$. Indeed, Fig. 7 shows that the h factor remarkably decreases near T_c. Thus, one needs to take a smaller value of the probing rate than $N_{\rm prob}/N=0.3$ to obtain single-particle properties of a uniform Fermi gas at $T\simeq T_c$.

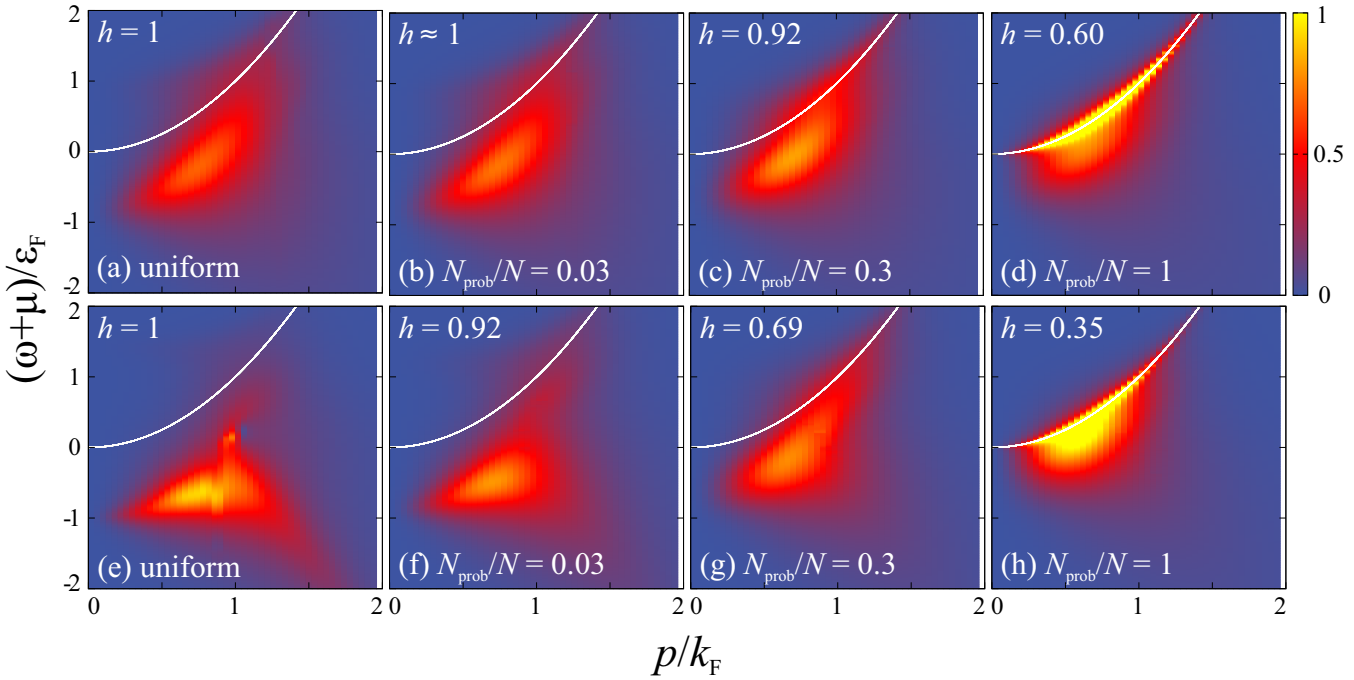

FIG. 6. (a)–(d) Calculated local photoemission spectra when $(k_F a_s)^{-1} = 0.1$ and $T = 1.24T_c$. (a) Uniform case. (b) $N_{prob}/N = 0.03$. (c) $N_{prob}/N = 0.3$. (d) $N_{prob}/N = 1$. The case in (d) is the same as the conventional photoemission spectrum $I_{PES}(\boldsymbol{p},\omega)$, where all the atoms in the trap contribute to the spectrum. (e)–(h) Same plots as (a)–(d), but in the unitarity limit $[(k_F a_s)^{-1} = 0]$ at T_c. The white solid line shows the free-particle dispersion.

The decrease in h near T_c is related to the pseudogap phenomenon appearing in the central region of a trapped Fermi gas. To see this, it is convenient to introduce the LDA *local* Fermi temperature $T_F(\boldsymbol{r})$, given by

$$T_F(\boldsymbol{r}) = \varepsilon_F - V(\boldsymbol{r}) \quad [\varepsilon_F \geqslant V(\boldsymbol{r})]. \tag{27}$$

Equation (27) is a natural extension of the ordinary Fermi temperature to the LDA case with the position-dependent Fermi chemical potential $\mu(\boldsymbol{r}) = \mu - V(\boldsymbol{r})$. In Eq. (27), the Fermi energy $\varepsilon_F = [3\pi^2 n(0)]^{2/3}/(2m)$ involves the particle density $n(0)$ of a trapped free Fermi gas at $\boldsymbol{r} = \boldsymbol{0}$. When the temperature is scaled as $T/T_F(\boldsymbol{r})$, it increases with distance from the trap center, as shown in Fig. 8. Because of this, even when strong pairing fluctuations cause pseudogapped single-particle excitations in the trap center below the so-called pseudogap temperature T_{pg} [53,71], pairing fluctuations are still weak in the outer region of the gas cloud where $T/T_F(\boldsymbol{r}) > T_{pg}/T_F(0)$, leading to the vanishing pseudogap phenomenon there. This naturally gives the coexistence of the pseudogapped central region and the outer region with no pseudogapped local density of states.

When $T_c \leqslant T \leqslant T_{pg}$, such spatial inhomogeneity would remarkably decrease h from unity, unless the pseudogapped region spreads out over the entire spatial region where LPES observes atoms. In the case of Fig. 3 ($N_{prob}/N = 0.3$), the size of the spatial region where LPES observes atoms is as large as about half the Thomas-Fermi radius R_F. We briefly note that, even at T_c, the pseudogapped spatial region is not so spread out in the unitary regime [72]. As a result, single-particle properties are still inhomogeneous in the region where LPES observes atoms, leading to the decrease in h.

When $T > T_{pg}$, the spatial inhomogeneity of the pseudogap phenomenon no longer exists. Because of this, a large value of h ($\simeq 1$) is expected compared to the pseudogapped case, which causes the difference between Figs. 6(c) and 6(g).

Although there is no clear boundary regarding the validity of the current LPES experiment (with $N_{prob}/N \simeq 0.3$), it is convenient to introduce the quantity $T^*(N_{prob}/N = 0.3)$, which is given as the temperature at which the h factor reaches $h = 0.9$ [see Fig. 7(b)]. As a criterion, we then identify the region above T^* (where $h \geqslant 0.9$) as the region where LPES can (approximately) eliminate the effects of a harmonic trap from photoemission spectra.

Using this criterion, we conveniently identify the region where the current LPES experiment ($N_{prob}/N = 0.3$) works, as shown in Fig. 9. In this figure, we see that most of the pseudogap regime ($T_c \leqslant T \leqslant T_{pg}$) is outside this region. Thus, the current LPES experiment with $N_{prob}/N \gtrsim 0.3$ needs further improvement to confirm the pseudogap phenomenon in the BCS-BEC-crossover regime of a *uniform* Fermi gas. At present, it seems difficult to select a narrower spatial region to give a larger h because of the limitation of the detectable spectral intensity in the current experimental technology [29]. Thus, a promising idea is to combine the current LPES technique with the nonharmonic (box-type and cylindrical) trap potential [27,28] mentioned in Sec. I. Then, the spatial inhomogeneity inside the selected region would be suppressed to some extent.

IV. SUMMARY

To summarize, we have discussed single-particle excitations in the BCS-BEC-crossover regime of a trapped ultracold

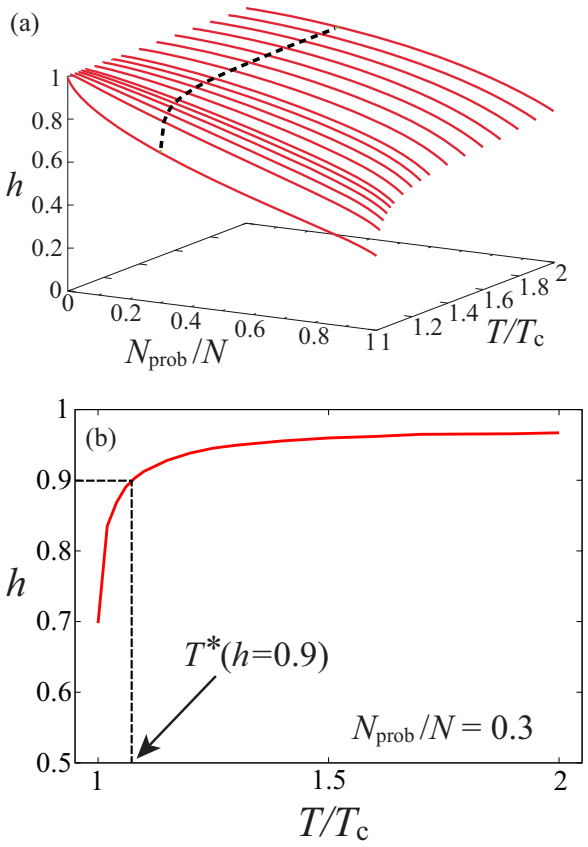

FIG. 7. (a) Calculated h factor in Eq. (24) as a function of the temperature T and the probing rate $N_{\rm prob}/N$. We take $(k_{\rm F}a_s)^{-1} = 0$. The dotted line shows the result at $N_{\rm prob}/N = 0.3$, which is also shown in (b) the two-dimensional panel for clarity. In (b) $T^*(h = 0.9)$ is the temperature above which $h \geqslant 0.9$ is realized. In this panel, the lowest temperature equals $T_{\rm c}$.

Fermi gas. Including pairing fluctuations within a strong-coupling T-matrix approximation, as well as the effects of the trapping potential using the local-density approximation, we have calculated the local photoemission spectrum $I_{\rm LPES}(\boldsymbol{p},\omega)$ in the normal state above $T_{\rm c}$. We showed that our results agree well with the recent local photoemission spectroscopy

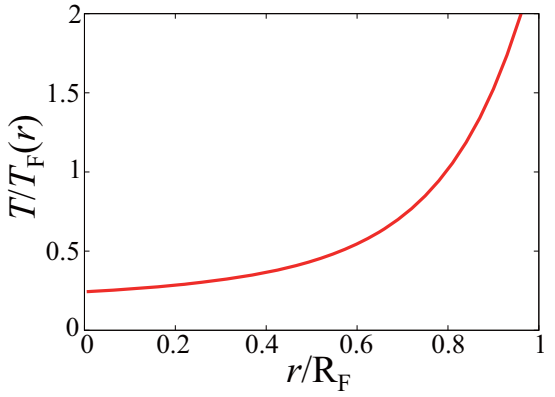

FIG. 8. Scaled local temperature $T/T_{\rm F}(\boldsymbol{r})$ at the unitary $(k_{\rm F}a_s)^{-1} = 0$.

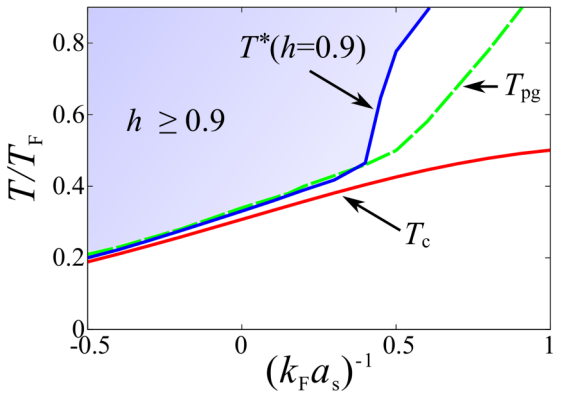

FIG. 9. Temperature T^* above which $h \geqslant 0.9$ is realized when $N_{\rm prob}/N = 0.3$ in the BCS-BEC-crossover regime of a trapped ultracold Fermi gas. $T_{\rm pg}$ is the pseudogap temperature [53] at which a dip structure (pseudogap) starts to appear in the single-particle density of state at the trap center. In the region $T_{\rm c} \leqslant T \leqslant T_{\rm pg}$, the single-particle density of states around the trap center has a gaplike structure in spite of the normal state.

experiment on a ^{40}K Fermi gas without introducing any fitting parameter. To conveniently estimate the similarity between the observed photoemission spectrum in a trapped Fermi gas and that in the homogeneous case, we have introduced a quantity (referred to as the h factor in this paper) to show that the recently observed LPES spectra in the unitary regime of a trapped ^{40}K Fermi gas are very close to those in a uniform Fermi gas.

However, we also found that the current LPES experiment (which requires the probing rate $N_{\rm prob}/N \gtrsim 0.3$ to obtain detectable spectral intensity) does not always work well for the purpose of eliminating the effects of a harmonic trap from the spectrum. In particular, we showed that the h factor remarkably deviates from unity in most of the pseudogap regime when $N_{\rm prob}/N \gtrsim 0.3$, which means that the current photoemission spectrum still involves the effects of spatial inhomogeneity there. Thus, in order to use LPES to resolve the debate about the existence of the pseudogap in the BCS-BEC-crossover regime of a uniform Fermi gas, it is necessary to improve this experiment beyond the current limitation ($N_{\rm prob}/N \gtrsim 0.3$).

For this improvement, one needs either to observe a smaller spatial region around the trap center or to use another type of trap potential. In this regard, the recent experimental work on nonharmonic traps [27,28] is promising. Since it gives a flatter potential than the ordinary harmonic potential in the central region, the LPES combined with such a nonharmonic trap may enable us to obtain the photoemission spectrum with $h \simeq 1$ within the current experimental limitation ($N_{\rm prob}/N \gtrsim 0.3$). Theoretical confirmation of this expectation is an interesting future problem. Extracting homogeneous information about a strongly interacting Fermi gas from experiments on a trapped Fermi gas is an important issue in cold Fermi gas physics, especially when this highly tunable system is used as a quantum simulator for other *homogeneous* Fermi systems. Thus, our results would be useful when such an application is intended for the study of single-particle excitations.

ACKNOWLEDGMENTS

We acknowledge T. E. Drake for providing us with the experimental data in Fig. 6. This work was supported by the KiPAS project at Keio University. D.I. was supported by a Grant-in-aid for Scientific Research from JSPS in Japan (Grant No. JP16K17773). Y.O. was supported by a Grant-in-aid for Scientific Research from JSPS in Japan (Grants No. JP15H00840, No. JP15K00178, and No. JP16K05503).

[1] Q. Chen, J. Stajic, S. Tan, and K. Levin, Phys. Rep. **412**, 1 (2005).
[2] I. Bloch, J. Dalibard, and W. Zwerger, Rev. Mod. Phys. **80**, 885 (2008).
[3] S. Giorgini, L. P. Pitaevskii, and S. Stringari, Rev. Mod. Phys. **80**, 1215 (2008).
[4] C. Chin, R. Grimm, P. Julienne, and E. Tiesinga, Rev. Mod. Phys. **82**, 1225 (2010).
[5] E. Timmermans, K. Furuya, P. W. Milonni, and A. K. Kerman, Phys. Lett. A **285**, 228 (2001).
[6] C. A. Regal, M. Greiner, and D. S. Jin, Phys. Rev. Lett. **92**, 040403 (2004).
[7] M. W. Zwierlein, C. A. Stan, C. H. Schunck, S. M. F. Raupach, A. J. Kerman, and W. Ketterle, Phys. Rev. Lett. **92**, 120403 (2004).
[8] M. Bartenstein, A. Altmeyer, S. Riedl, S. Jochim, C. Chin, J. H. Denschlag, and R. Grimm, Phys. Rev. Lett. **92**, 203201 (2004).
[9] J. Kinast, S. L. Hemmer, M. E. Gehm, A. Turlapov, and J. E. Thomas, Phys. Rev. Lett. **92**, 150402 (2004).
[10] P. Nozières and S. Schmitt-Rink, J. Low Temp. Phys. **59**, 195 (1985).
[11] C. A. R. Sá de Melo, M. Randeria, and J. R. Engelbrecht, Phys. Rev. Lett. **71**, 3202 (1993).
[12] M. Randeria, in *Bose-Einstein Condensation*, edited by A. Griffin, D. W. Snoke, and S. Stringari (Cambridge University Press, New York, 1995), p. 355.
[13] Y. Ohashi and A. Griffin, Phys. Rev. Lett. **89**, 130402 (2002).
[14] A. Perali, P. Pieri, G. C. Strinati, and C. Castellani, Phys. Rev. B **66**, 024510 (2002).
[15] P. Pieri, L. Pisani, and G. C. Strinati, Phys. Rev. B **70**, 094508 (2004).
[16] W. Ketterle and M. W. Zwierlein, in *Ultra-cold Fermi Gases*, edited by M. Inguscio, W. Ketterle, and C. Salomon, Proceedings of the International School of Physics "Enrico Fermi" Vol. 164 (IOS Press, Amsterdam, 2008), pp. 95–287.
[17] *The BCS-BEC Crossover and the Unitary Fermi Gas*, edited by W. Zweger (Springer, Berlin, 2012).
[18] C. Renner, B. Revaz, J.-Y. Genoud, K. Kadowaki, and O. Fischer, Phys. Rev. Lett. **80**, 149 (1998).
[19] A. Perali, C. Castellani, C. D. Castro, M. Grilli, E. Piegari, and A. A. Varlamov, Phys. Rev. B **62**, R9295 (2000).
[20] A. Damascelli, Z. Hussain, and Z.-X. Shen, Rev. Mod. Phys. **75**, 473 (2003).
[21] Q. Chen, K. Levin, and J. Stajic, J. Low Temp. Phys. **32**, 406 (2006).
[22] D. J. Dean and M. Hjorth-Jensen, Rev. Mod. Phys. **75**, 607 (2003).
[23] T.-L. Ho and Q. Zhou, Nat. Phys. **6**, 131 (2010).
[24] N. Navon, S. Nascimbène, F. Chevy, and C. Salomon, Science **328**, 729 (2010).
[25] M. J. Ku, A. T. Sommer, L. W. Cheuk, and M. W. Zwierlein, Science **335**, 563 (2012).
[26] M. Horikoshi, M. Koashi, H. Tajima, Y. Ohashi, and M. Kuwata-Gonokami, arXiv:1612.04026.
[27] A. L. Gaunt, T. F. Schmidutz, I. Gotlibovych, R. P. Smith, and Z. Hadzibabic, Phys. Rev. Lett. **110**, 200406 (2013).
[28] B. Mukherjee, Z. Yan, P. B. Patel, Z. Hadzibabic, T. Yefsah, J. Struck, and M. W. Zwierlein, Phys. Rev. Lett. **118**, 123401 (2017).
[29] Y. Sagi, T. E. Drake, R. Paudel, R. Chapurin, and D. S. Jin, Phys. Rev. Lett. **114**, 075301 (2015).
[30] J. T. Stewart, J. P. Gaebler, and D. S. Jin, Nature (London) **454**, 744 (2008).
[31] J. P. Gaebler, J. T. Stewart, T. E. Drake, D. S. Jin, A. Perali, P. Pieri, and G. C. Strinati, Nat. Phys. **6**, 569 (2010).
[32] T. E. Drake, Y. Sagi, R. Paudel, J. T. Stewart, J. P. Gaebler, and D. S. Jin, Phys. Rev. A **86**, 031601 (2012).
[33] Y. Sagi, T. E. Drake, R. Paudel, and D. S. Jin, Phys. Rev. Lett. **109**, 220402 (2012).
[34] Y. Sagi, T. E. Drake, R. Paudel, R. Chapurin, and D. S. Jin, J. Phys. Conf. Ser. **467**, 012010 (2013).
[35] P. Törmä and P. Zoller, Phys. Rev. Lett. **85**, 487 (2000).
[36] P. Törmä, Phys. Scr. **91**, 043006 (2016).
[37] S. Tsuchiya, R. Watanabe, and Y. Ohashi, Phys. Rev. A **80**, 033613 (2009); **82**, 033629 (2010).
[38] R. Watanabe, S. Tsuchiya, and Y. Ohashi, Phys. Rev. A **82**, 043630 (2010).
[39] H. Hu, X.-J. Liu, P. D. Drummond, and H. Dong, Phys. Rev. Lett. **104**, 240407 (2010).
[40] C.-C. Chien, H. Guo, Y. He, and K. Levin, Phys. Rev. A **81**, 023622 (2010).
[41] A. Perali, F. Palestini, P. Pieri, G. C. Strinati, J. T. Stewart, J. P. Gaebler, T. E. Drake, and D. S. Jin, Phys. Rev. Lett. **106**, 060402 (2011).
[42] Q. Chen and J. Wang, Front. Phys. **9**, 539 (2014).
[43] F. Palestini, A. Perali, P. Pieri, and G. C. Strinati, Phys. Rev. B **85**, 024517 (2012).
[44] S. Nascimbène, N. Navon, S. Pilati, F. Chevy, S. Giorgini, A. Georges, and C. Salomon, Phys. Rev. Lett. **106**, 215303 (2011).
[45] S. Nascimbène, N. Navon, K. J. Jiang, F. Chevy, and C. Salomon, Nature (London) **463**, 1057 (2010).
[46] M. Randeria, N. Trivedi, A. Moreo, and R. T. Scalettar, Phys. Rev. Lett. **69**, 2001 (1992).
[47] J. M. Singer, M. H. Pedersen, T. Schneider, H. Beck, and H.-G. Matuttis, Phys. Rev. B **54**, 1286 (1996).
[48] B. Jankó, J. Maly, and K. Levin, Phys. Rev. B **56**, R11407 (1997).
[49] Y. Yanase and K. Yamada, J. Phys. Soc. Jpn. **70**, 1659 (2001).
[50] D. Rohe and W. Metzner, Phys. Rev. B **63**, 224509 (2001).
[51] G. D. Mahan, *Many-Particle Physics* (Plenum, New York, 1981).
[52] G. Rickayzen, *Green's Functions and Condensed Matter* (Dover, New York, 2013).
[53] S. Tsuchiya, R. Watanabe, and Y. Ohashi, Phys. Rev. A **84**, 043647 (2011).

[54] D. S. Petrov, C. Salomon, and G. V. Shlyapnikov, Phys. Rev. Lett. **93**, 090404 (2004).
[55] P. Pieri and G. C. Strinati, Phys. Rev. B **71**, 094520 (2005).
[56] T. Kashimura, R. Watanabe, and Y. Ohashi, Phys. Rev. A **86**, 043622 (2012).
[57] G. M. Bruun, P. Törmä, M. Rodriguez, and P. Zoller, Phys. Rev. A **64**, 033609 (2001).
[58] J. Kinnunen, M. Rodríguez, and P. Törmä, Science **305**, 1131 (2004).
[59] Y. He, Q. Chen, and K. Levin, Phys. Rev. A **72**, 011602 (2005).
[60] Q. Chen, Y. He, C.-C. Chien, and K. Levin, Rep. Prog. Phys. **72**, 122501 (2009).
[61] Y. Ohashi and A. Griffin, Phys. Rev. A **72**, 013601 (2005).
[62] D. A. Butts and D. S. Rokhsar, Phys. Rev. A **55**, 4346 (1997).
[63] Y. Ohashi and A. Griffin, Phys. Rev. A **67**, 033603 (2003).
[64] We assume that $|\uparrow\rangle$ and $|3\rangle$ feel the same trap potential $V(\boldsymbol{r})$ for simplicity.
[65] In LDA, the case of an anisotropic trap $V(\boldsymbol{r}) = m\sum_{i=x,y,z}\omega_i^2 r_i^2/2$ can be always transformed to the isotropic case by simply rescaling the spatial variables as $r_i \to (\omega_{\rm tr}/\omega_i)r_i$. Thus, we deal only with the isotropic case in this paper.
[66] C. J. Pethick and H. Smith, *Bose-Einstein Condensation in Dilute Gases* (Cambridge University Press, Cambridge, 2002).
[67] In Ref. [29], each hollow light beam gives $P(\boldsymbol{r})$ in Eqs. (18) and (19), where r is replaced by the distance $r_\perp$ from the beam axis.
[68] H. J. Vidberg and J. W. Serene, J. Low Temp. Phys. **29**, 179 (1977).
[69] K. S. D. Beach, R. J. Gooding, and F. Marsiglio, Phys. Rev. B **61**, 5147 (2000).
[70] D. J. Thouless, Ann. Phys. (N.Y.) **10**, 553 (1960).
[71] The pseudogap temperature $T_{\rm pg}$ in LDA is determined as the temperature at which the single-particle density of states at $\boldsymbol{r} = 0$ starts to have a dip structure around $\omega = 0$ [53].
[72] R. Watanabe, S. Tsuchiya, and Y. Ohashi, Phys. Rev. A **86**, 063603 (2012).